International Journal of Fluid Machinery and Systems
Vol. 9, No. 1, January-March 2016

DOI: http://dx.doi.org/10.5293/IJFMS.2016.9.1.095
ISSN (Online): 1882-9554

Original Paper

Optimization of Blade Profile of a Plenum Fan

Lin Wu[1], Hua-Shu Dou[1], Yikun Wei[1], Yongning Chen[2], Wenbin Cao[2], Cunlie Ying[2]

[1]Faculty of Mechanical Engineering and Automatic, Zhejiang Sci-Tech University
5 Second Avenue, Xiasha Higher Education Zone, Hangzhou, 310018, China
wulin_1991@yahoo.com, huashudou@yahoo.com, ykun-wei@sina.com
[2]Zhejiang Yilida Ventilator CO., Ltd
Hengjie, Luqiao District, Taizhou, 318056, China
cyn121@yilida.com, caowenbin@yilida.com, yingcunlie@yilida.com

Abstract

A method of optimization design for the blade profile of a centrifugal impeller by controlling velocity distribution is presented, and a plenum fan is successfully designed. This method is based on the inner flow calculation inside the centrifugal impeller, and is related to the distribution of relative velocity. The results show that after optimization, the boundary layer separation on the suction surface has been inhibited and the stability of plenum fan is improved. The flow at the impeller outlet is also studied, and the jet-wake pattern at the impeller outlet is improved obviously by optimization. The calculation result shows that the static pressure and static pressure efficiency can be increased by 15.4% and 21.4% respectively.

Keywords: velocity distribution, blade profile, static pressure, static pressure efficiency

1. Introduction

Impeller is the core component of the centrifugal fan, and the impeller loss is the main source of the fan loss. The impeller performance directly determines the performance of the fan, so an approach to improve the aerodynamic performance of centrifugal fan is important in designing a high-performance centrifugal impeller. Traditional design methods such as semi-blades [1] [2], using external devices [3], and changing structure [4] often rely on the engineering experience, which limits the fan performance. Some advanced design methods like loss model [5] and genetic algorithm [6] are better, but they require huge database and high computational cost due to the mathematical model they based on

In a centrifugal fan impeller, the blade is one of the most important parts. The blade plays a decisive role in the internal flow and the fan performance. The velocity distribution on the blade surface is closely related to the inner flow of centrifugal fan. The boundary layer separation and secondary flow are influenced by the velocity distribution as well. As the development of research method, the understanding of the inner flow in centrifugal impeller is clearer, and it provides a feasible way to optimize the centrifugal impeller.

In the NACA report, Stanitz et al [7] pointed out that the boundary layer of blade surface will affect the impeller viscous losses directly, and the growth of the boundary layer is related to the speed on lateral of the boundary layer. The separation may occur when the speed decelerate quickly, thus causing loss. Johnson [8] studied the velocity distribution on the centrifugal compressor blade, and the theoretical analysis proceeded by giving four kinds of velocity distribution. The results show that the secondary flow is improved under the linear load, and the bilinear load can reduce the velocity gradient, then the boundary layer separation and growth is inhibited. Galerkin [9] studied the centrifugal impeller performance by given three typical velocity distributions in experiment. The result shows that the impeller can obtain the best performance using the C velocity distribution. Balje et al [10] studied the boundary layer momentum thickness under the influence of velocity distribution based on the theory of boundary layer. The research shows that the faster the deceleration on the initial of the blade, the thinner the boundary layer momentum thickness.

There are some research progress in designing the impeller and blade. Qi et al [11] presented a simple two-dimensional inverse design method, and the experiment was processed to study the reasonable relative velocity distribution. The result shows that the best performance can be obtained when the deceleration form is slow-rapid-slow. This method is applied in a plate blade optimization process and obtains an obvious effect. Li et al [12] assumed that the average relative velocity distribution alongside

Received November 30 2015; accepted for publication December 19 2015: Review conducted by Tadashi Tanuma, Ph.D. (Paper number O15074S)
Corresponding author: Hua-Shu Dou, huashudou@yahoo.com
This paper was presented at 13th Asian International Conference on Fluid Machinery (AICFM), September 7-10, 2015, Tokyo, Japan

the streamline in channel is cubic polynomial, and redesigned the centrifugal fan using optimized velocity distribution. The optimization process changes the forward fan into a back-ward fan, and the pressure and efficiency are improved. Shibata [13] [14] researched the effect of different load on surge by presenting three kinds of centrifugal compressor impeller blade load distribution. The load distribution was expressed by piecewise function, and velocity distribution was calculated accordingly. Lin S C [15] studied the performance of centrifugal fan used in notebook computer based on NACA4412 airfoil. The results show that the velocity distribution of flow channel is relatively reasonable, and the jet-wake pattern is inhibited.

In this paper, the blade profile of a centrifugal impeller is designed by controlling velocity distribution. Static pressure and static efficiency from numerical simulation are well consistent with the experimental data at rated flow coefficient. Then the impeller parameters according to the design requirements are calculated. The boundary layer momentum thickness is obtained by Truckenbrodt equation, and the required parameters in the equation are from the velocity distribution curve in reference [9]. Then the reasonable velocity curve parameters are selected according to the minimum boundary layer momentum thickness. The relative velocity expression can be determined by the fan parameters and the reasonable velocity curve. Then the radial mean line of channel is obtained based on the relative velocity expression and the meridian section. The thickness distribution of NACA0010 is applied as the blade profile thickness. The simulation of optimized model is carried out and the comparison with the original fan is performed. Measurements of static pressure, static efficiency, and velocity at different flow coefficients are conducted for both original and optimized fan. At last details of the inner flow are analyzed.

2. Governing Equation

The governing equations of gas for static parts are three-dimensional Reynolds averaged Navier-Stokes equation (RANS):

$$\nabla \cdot \vec{u} = 0 \tag{1}$$

$$\frac{\partial \vec{u}}{\partial t} + (\vec{u} \cdot \nabla)\ \vec{u} = -\frac{1}{\rho}\nabla p + \frac{\mu + \mu_t}{\rho}\nabla^2 \vec{u} \tag{2}$$

where $\vec{u}$ is the fluid velocity, ρ is the fluid density, μ and μ_t are the fluid viscosity and the turbulent viscosity respectively, and p is the pressure.

In rotating part, according to the relative velocity formulation, fluid velocities can be transformed from the stationary frame to the moving frame using the following relation:

$$\vec{v}_r = \vec{v} - \vec{u}_r \tag{3}$$

$$\vec{u}_r = \vec{\omega} \times \vec{r} \tag{4}$$

where $\vec{v}_r$ is the relative velocity (the velocity viewed from the rotating frame), $\vec{v}$ is the absolute velocity (the velocity viewed from the stationary frame), $\vec{u}_r$ is the velocity of the moving frame relative to the inertial reference frame, and $\vec{\omega}$ is the angular velocity.

Then, the governing equations (Eq. (1) and (2)) of fluid flow in a rotating reference frame can be written as follows:

Conservation of mass:

$$\Delta \cdot \rho \vec{v}_r = 0 \tag{5}$$

Conservation of momentum:

$$\Delta \cdot \left(\rho \vec{v}_r \vec{v}_r\right) + \rho\left(2\vec{\omega} \times \vec{v}_r + \vec{\omega} \times \vec{\omega} \times \vec{r}\right) = -\Delta p + \Delta \cdot \tau_r + \vec{F} \tag{6}$$

where τ_r is the total shear stress.

The SST k-omega model is selected as the turbulence model in this paper [14].

3. Numerical Investigation

3.1 Numerical methods

The finite volume method is adopted in this work, and the SIMPLEC algorithm is used for pressure and velocity coupling with secondary order upwind difference interpolation. It is necessary for a run to converge to satisfy the requirement of maximum residuals, or the differential pressure between inlet and outlet to be stable.

The inlet boundary is mass flow inlet and the outlet boundary is pressure outlet using atmosphere pressure. All solid walls are no-slip walls, and the rotating speed of the impeller is 1450 rpm as same as that in the experiment. The multiple rotating reference frames are employed in the calculation considering the static parts and the rotating part. The simulation is performed with steady calculation.

3.2 Geometrical model and mesh

The original model is a plenum fan numbered with SYW-560 produced by Zhejiang Yilida Company, as shown in Fig. 1(a). The whole computational geometry is shown in Fig. 1(b). The outer area of the computing domain is a cylinder whose diameter is 6 times the plenum fan diameter and the height is double of the width of the impeller. The inflow domain is a cylinder whose diameter is 5 times the plenum fan diameter, and the height is 20 times the plenum fan width. The static pressure is referred at the inlet and outlet, and the difference is the static pressure of the plenum fan. More details of the plenum fan are given in Table 1.

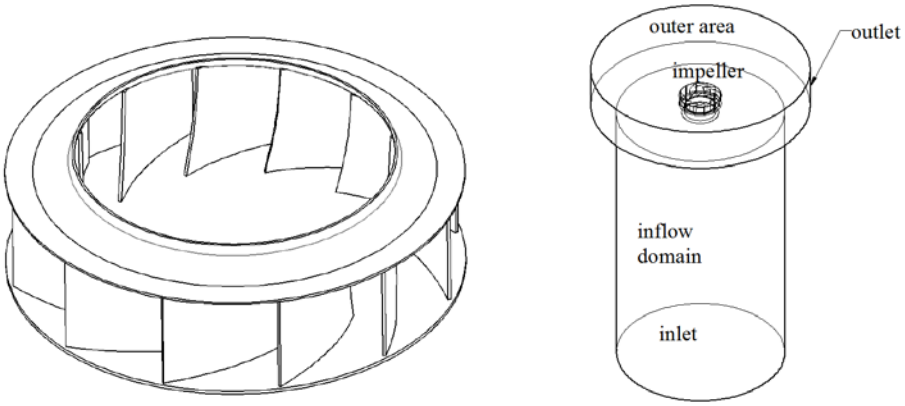

（a） the plenum fan impeller （b） the total geometry

Fig. 1 Plenum fan model

Table 1 Rated variables of plenum fan

Variables	units	value
Flow coefficient		0.198
Static pressure	Pa	632
Efficiency of static pressure	%	52.87
Revolving speed	rpm	1450
Impeller diameter	mm	570
Impeller outlet breadth	mm	133
Number of blades		12

The structured grid is used in the static parts, and the unstructured tetrahedral grid is used in rotating part. The total elements of the original model are about 4,600,000, and the elements of plenum fan are about 3,900,000. The axial section of grid is shown in Fig. 2.

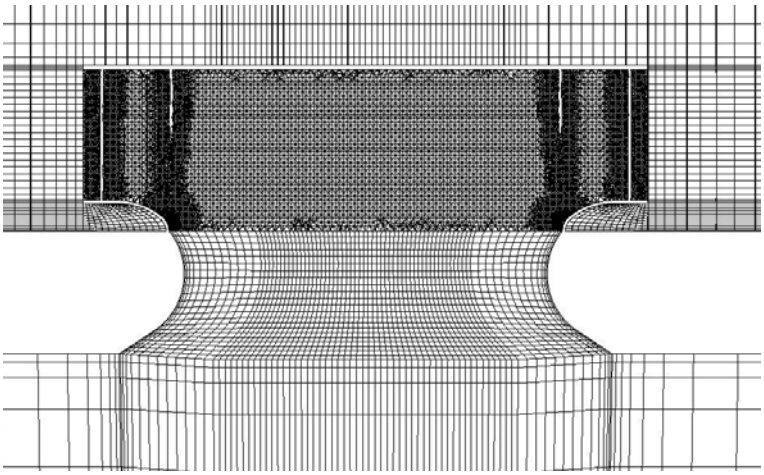

Fig. 2 Mesh system

4. Numerical Result of Original Fan

4.1 Mesh independence verification

Mesh independence verification for original model is performed to find an appropriate amount of mesh number. As is shown in Table 2, a 4,604,948 mesh system is sufficiently meet the requirements and is thus used in this paper (to satisfy the flow characteristics, and is thus utilized in present analysis).

Table 2 Comparison of used meshes

	Total	impeller	Static pressure
First mesh	3,022,544	1,508,642	627
Second mesh	3,808,712	2,294,810	613
Third mesh	4,604,948	3,091,046	609
Fourth mesh	5,204,749	3,590,847	609
Fifth mesh	6,734,251	5,220,349	608

4.2 Numerical methodology verification

Table 3 shows the comparison of static pressure of numerical simulation and experimental data at the rated flow coefficient. It

can be seen that the error is within permission, and the numerical methodology is reliable. The cause of the difference is due to that there is difference between the condition of experiment and the simplified model used for simulation. A tiny difference exists between the simulation results and experimental data.

Table 3 Comparison of static pressure

	Static pressure	Static efficiency
Experiment	632	52.87%
Numerical simulation	609	57.5%

5. Optimization procedure

The condition for the optimization is described as follow. The flow coefficient and the rotating speed are fixed, and the desired static pressure is set at 700pa. The dimensions of the impeller are fixed, and blade parameters are changed.

Based on the rated flow coefficient and the desired static pressure, the basic parameters of impeller can be calculated, as shown in Table 4.

Table 4 Basic parameters of the impeller

Parameter	Unit	Value
Outlet diameter	mm	578
Outlet width	mm	131
Blade outlet angle	degree	32
Blade inlet angle	degree	31
Blade outlet diameter	mm	572

The growth of the boundary layer results in energy loss and the separation of boundary layer at inverse pressure gradient leads to change of flow structure. It is desired to restrict the growth of boundary layer in the design of blade profile. Thus, the momentum thickness of the boundary layer should be controlled. The way to control the boundary layer momentum thickness is to control the relative velocity distribution. It is assumed that the relative velocity is the average of relative velocities on pressure and suction surface. According to the reference [9], the relative velocity curve is divided into three sections of smooth connection curves, and the functions of the three curves are quadratic, cubic, and quadratic respectively. Therefore, the four control points are the starting point, ending point and the two junctions of the three. As shown in Fig. 3, the abscissa expresses the blade length and the ordinate stands for the relative velocity.

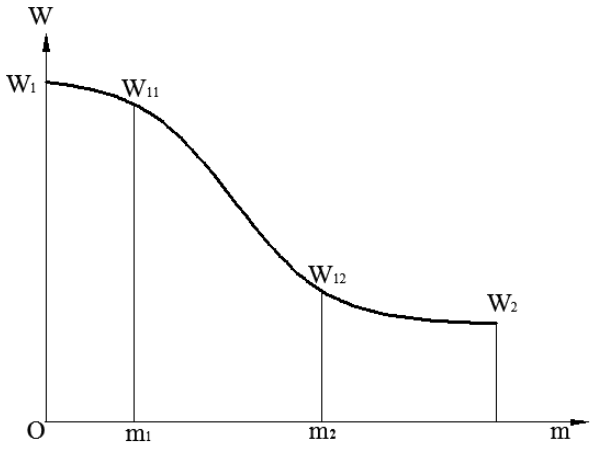

Fig. 3 Relative velocity along the flow distance

The coordinate of the four control points are (0, W_1), (m_1, W_{11}), (m_2, W_{12}) and (m_0, W_2). Two reduction ratios $U_1=W_1/W_{11}$, $U_2=W_1/W_{12}$ are defined, in which the starting velocity W_1 and the ending velocity W_2 can be calculated using the following equations. The function of each curve can be determined.

$$\omega_1 = \frac{Q_T}{\pi D_1 b_1 \mu \sin \beta_{b1} \tau_1} \tag{10}$$

$$\omega_2 = \frac{Q_T}{\sin \beta_{b2} \pi D_2 b_2 \mu_2 \tau_2} \tag{11}$$

There is no method to get the accurate value of m_1, and 0.2 times of the blade length is usually used. The values of m_2, U_1 and U_2 are shown in Table 5.

Table 5 Values of m_2, U_1 and U_2

Variable				
m_2	0.6	0.7	0.8	0.9
U_1	1.02	1.03	1.04	1.05
U2	1.26	1.29	1.32	1.35

There exists pressure gradient in the blade channel. The Truckenbrodt equation is employed to calculate the boundary layer momentum thickness. For convenience, the relative velocity curve is split into three straight lines, and the equation is derived as follows:

$$\frac{\theta_2}{l}=\frac{\left(\frac{A}{4+\frac{2}{n}}\right)^{\frac{n}{n+1}}}{\mathrm{Re}^{\frac{1}{n+1}}}\left\{\frac{x_1\mu\left[\left(\frac{\alpha^*}{\mu}\right)^{\left(4+\frac{2}{n}\right)}-\left(\frac{1}{\mu}\right)^{\left(4+\frac{2}{n}\right)}\right]}{\alpha^*-1}-\frac{(x_2-x_1)\left[\beta^{*\left(4+\frac{2}{n}\right)}-\left(\frac{\alpha^*}{\mu}\right)^{\left(4+\frac{2}{n}\right)}\right]}{\frac{\alpha*}{\mu}-\beta^*}+\frac{(1-x_2)\left[1-\beta^{*\left(4+\frac{2}{n}\right)}\right]}{1-\beta^*}\right\}^{\left(\frac{n}{n+1}\right)} \tag{12}$$

where $\alpha^*=\frac{W11}{W1}$, $\beta^*=\frac{W12}{W2}$, $x_1=\frac{l_1}{l}$, $x_2=\frac{l_2}{l}$, and $\mu=\frac{W2}{W1}$.

According to the different permutation of the variables, 64 values of boundary layer momentum thickness are obtained by the calculation. In order to obtain a more accurate consequence, four minimum values are selected because the Truckenbrodt equation doesn't include the curvature and rotation. The control points of the four different groups are shown in Table 6.

Table 6 Control points and boundary layer momentum thickness

No.	m_2	U_1	U_2	The boundary layer momentum thickness
A	0.6	1.05	1.35	0.003869
B	0.6	1.04	1.35	0.003914
C	0.6	1.05	1.32	0.003944
D	0.6	1.03	1.35	0.00396

Then four velocity distribution functions can be obtained, and the accurate curves are shown in Fig. 4.

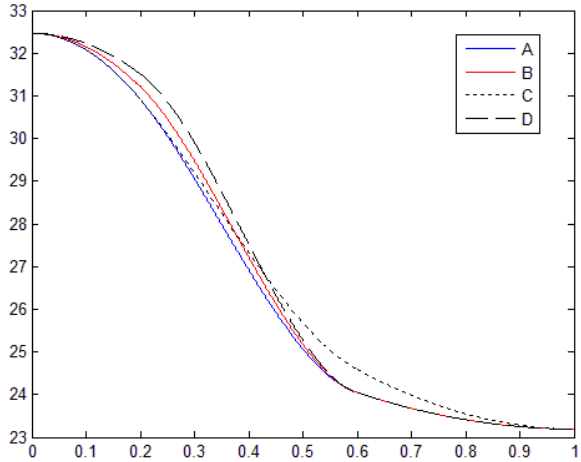

Fig. 4 Four relative velocity curves

Under this condition, the shroud and hub curve are fixed, and the blade angle at any radius can be obtained by the following equation:

$$\beta_b=\arcsin\left(\frac{Q_n}{2\pi Rb_r\tau\omega}\right) \tag{13}$$

where τ is the edge-thickness coefficient. The value of τ is based on τ_1 (blade inlet) and τ_2 (blade outlet). The value of τ_1 and τ_2 can be obtained by the following equation:

$$\tau_1=\frac{t_1-\delta_1/\sin\beta_{b1}}{t_1}=\frac{\frac{0.31\pi}{12}-\frac{0.004}{\sin 31}}{\frac{0.31\pi}{12}}=0.9073 \tag{14}$$

$$\tau_2=\frac{t_2-\delta_2/\sin\beta_{b2}}{t_2}=\frac{\frac{0.572\pi}{12}-\frac{0.004}{\sin 32}}{\frac{0.572\pi}{12}}=0.9521 \tag{15}$$

where t_1 and t_2 are the cascade spacing, which can be obtained by the following equation:

$$t=\frac{D\pi}{Z} \tag{16}$$

Setting i=1 at the entrance of the blade, and the centre angle φ is zero. The blade curve can be obtained by radius and the relevant φ, as shown in Fig. 5, and Fig. 6 shows the comparison. The value of $\Delta\varphi$ is obtained by the following equation:

$$\Delta\varphi^{\circ} = \frac{90}{\pi}\left(\frac{1}{R_i \tan\beta_{bi}} + \frac{1}{R_{i+1}\tan\beta_{bi+1}}\right)\Delta R_i \tag{17}$$

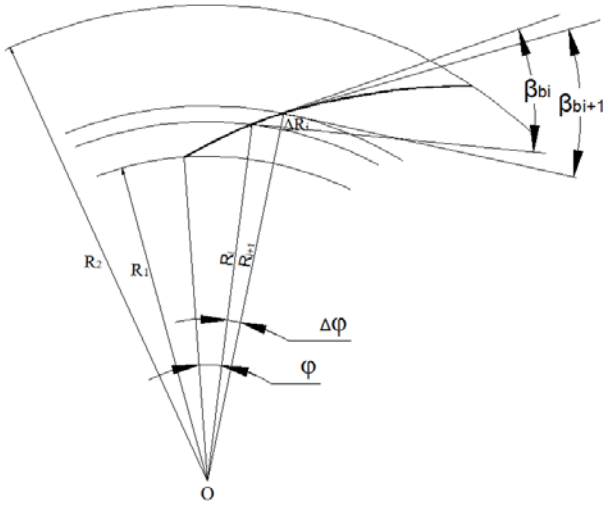

Fig. 5 Drawing method of blade curve

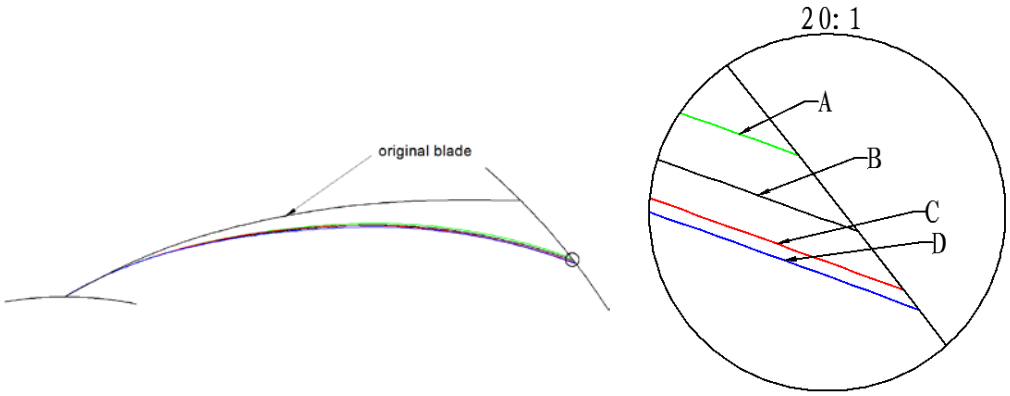

(a) comparison of different blade curves (b) local comparison

Fig. 6 Comparison of different blade curves

The 3D model based on the four blade curves are built respectively, and the simulation consequence of every model are shown in Table 7.

Table 7 Simulation of different models

Model name	Static pressure	Static pressure efficiency
Original model	609	57.5%
Model A	751	64.8%
Model B	719	63.2%
Model C	735	64.1%
Model D	730	63.7%

As it can be seen that the highest static pressure and static pressure efficiency is obtained with model A, the model A is selected as the mean line of the airfoil. The generation of asymmetric airfoil is to superpose the same thickness on both sides of the mean line, as shown in Fig. 7.

According to some design experience of the company, the reasonable thickness of wing blade is 10% of the blade chord length. Then the thickness distribution for NACA0010 is selected to get the wing section, and its function is as follows:

$$y_t = \frac{t}{0.2}(0.29690\sqrt{c} - 0.12600c - 0.35160c^2 + 0.28430c^3 - 0.10150c^4 \tag{18}$$

where t is the maximum thickness expressed as a fraction of the chord, c is the location of the chord. Here, $t = 1$.

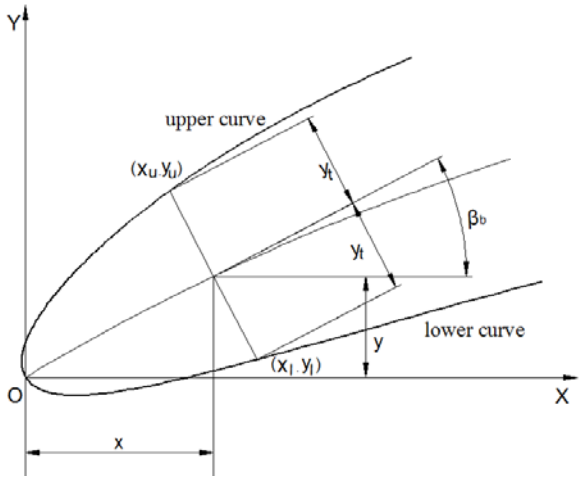

Fig. 7 Drawing method of asymmetric airfoil

The functions of the blade profile are:

$$x_u = x - 224.443 y_t \sin\beta_b \tag{19}$$

$$y_u = y + 224.443 y_t \cos\beta_b \tag{20}$$

$$x_l = x + 224.443 y_t \sin\beta_b \tag{21}$$

$$y_l = y - 224.443 y_t \cos\beta_b \tag{22}$$

where the subscript *u* means the upper curve and the subscript *l* means the lower curve.

6. Numerical Results and Discussion

6.1 Mesh independence verification

Based on the existing literature and engineering experience, the number of blade is usually between 6 and 9. The number of blades is set as 7, and the mesh independence verification of this model is carried out. It can be seen in the Table 8, when the total elements beyond 5,147,311 the change of static pressure is small.

Table 8 Mesh independence verification of optimized model

	Total	impeller	Static pressure
1	3,812,115	2,663,624	715
2	4,439,697	3,291,206	691
3	5,147,311	3,998,820	683
4	5,735,637	4,587,146	682

6.2 Blades number determination

The number of blades is determined by numerical simulation, and the mesh setting of different models is the same as the model with 7 blades. The result in Table 9 shows that the highest efficiency can be obtained at the model with 7 blades, but the static pressure is lower than desired. Considering the desired static pressure and static pressure efficiency, the blade number of 8 is selected.

Table 9 Comparison of performance with different number of blade

Number of blades	6	7	8	9
meshes	4844288	5147311	5401660	5718699
Static pressure	646	683	703	728
Static pressure efficiency	69.3%	70.2%	69.8%	68.3%

6.3 Comparison of the performance of the original and optimized model

Figure 8 shows the comparison of the performance of the original and optimized models. It can be seen in Fig. 8 that the static pressure and static pressure efficiency of the optimized model is higher than that of the original model at small and rated flow coefficient. But at the high flow coefficient, the performance of original model is better than the optimized model. The reason is that the blade outlet angle becomes small after optimization.

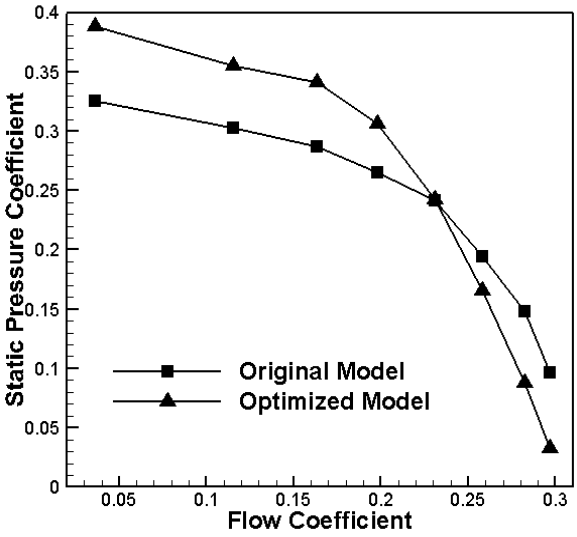

(a) Comparison of static pressure of original model and optimized model

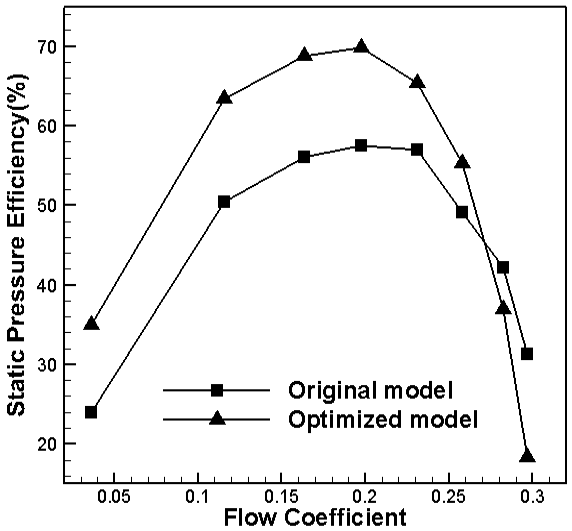

(b) Comparison of static efficiency of original model and optimized model

Fig. 8 Comparison of performance of the original and optimized model

Figure 9 shows the static pressure distribution of the middle section of both original and optimized model channels. It can be seen that in the optimized model, the increase of static pressure in the channel is more uniform and stable. The layering of the static pressure contour of optimized model is more obvious, and the loss on the blade outlet is less than that of the original model.

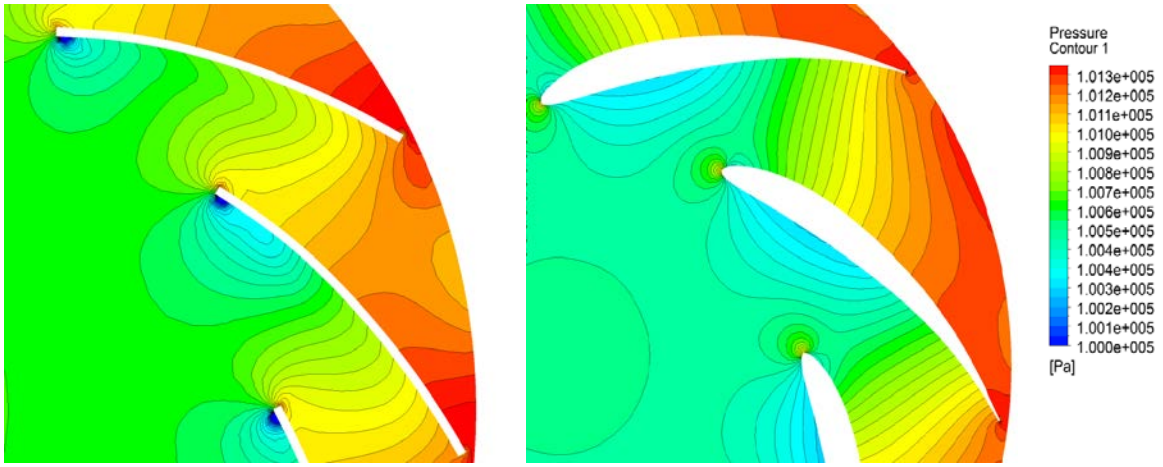

(a) Original Model (b) Optimized Model

Fig. 9 Static pressure distribution at the rated flow coefficient

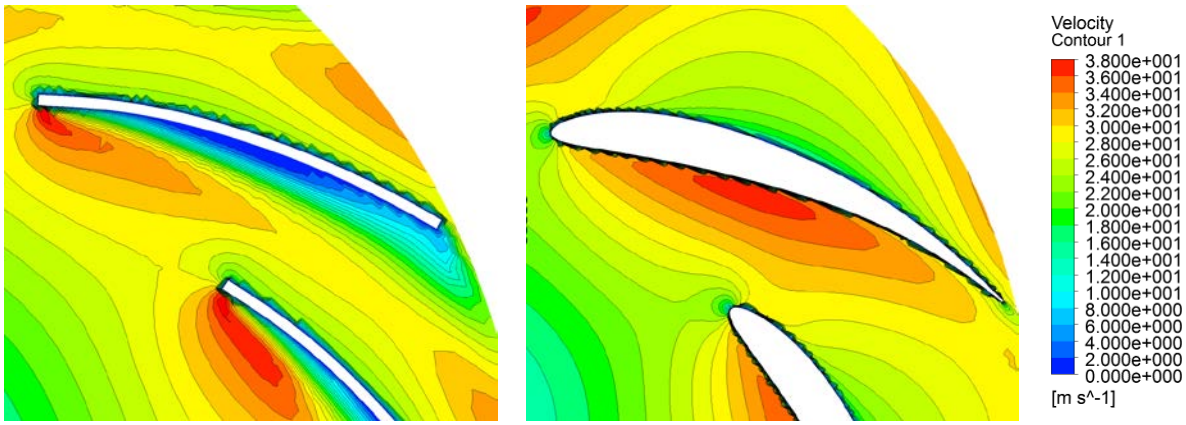

（a）Original model （b）Optimized Model

Fig. 10 Relative velocity distribution at the rated flow coefficient

Figure 10 presents the relative velocity distribution of middle section of both original and optimized model. It can be seen that there is obvious low velocity region on the suction surface in the original model. The low velocity region near the wall can be taken as boundary layer. In the optimized model, the low velocity region is far less, and this means that the boundary layer thickness of optimized model is thinner than that of the original model. The thicker boundary layer may cause the separation. Besides, because the fluid friction mainly occurs inside the boundary layer, the thicker boundary will lead more loss.

Because the flow separation always happens on the suction surface, analysis of the flow on the suction surface of both original

and optimized modals is presented. Figure 11 shows the comparison of streamline on the suction surface. It can be seen that in the original model, there is obvious vortex on the suction surface. Because the flow is unsteady in original model, the pattern of streamline is different on each blade. But in the optimized model, the flow is stable.

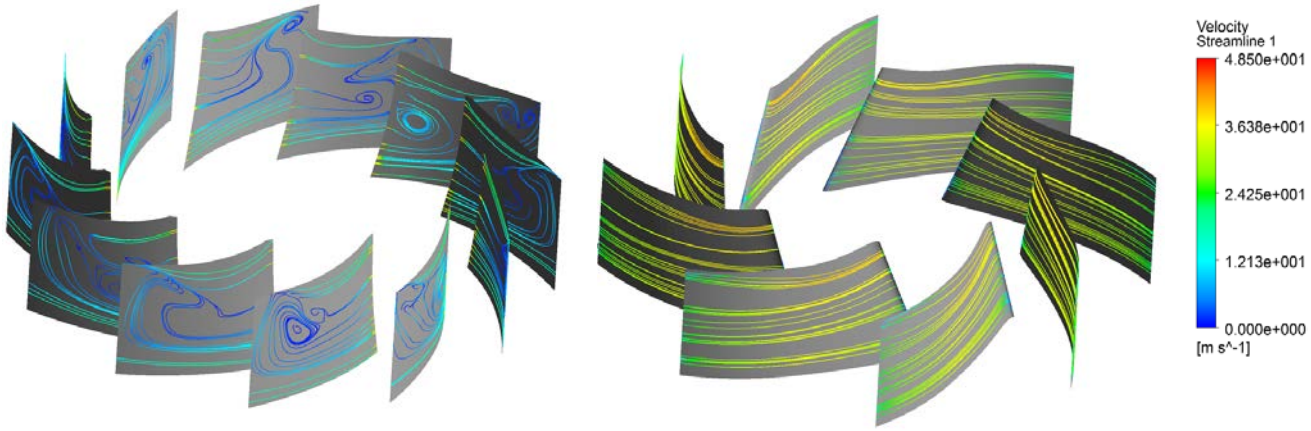

(a) Original Model (b) Optimized Model

Fig. 11 Suction surface streamline at the rated flow coefficient

Figure 12 is the vortices contour of the original and optimized model. It can be seen from Fig. 12(a), in the original case, vortex occurs mainly on the suction surface of blade. Speciously, at both ends of the blade, large scale vortex could be observed. However, Fig. 12(b) shows that only small vortex appears at both ends of the blade in the optimized case. Above all, the characteristic of inner flow in the fan is significantly improved after optimizing.

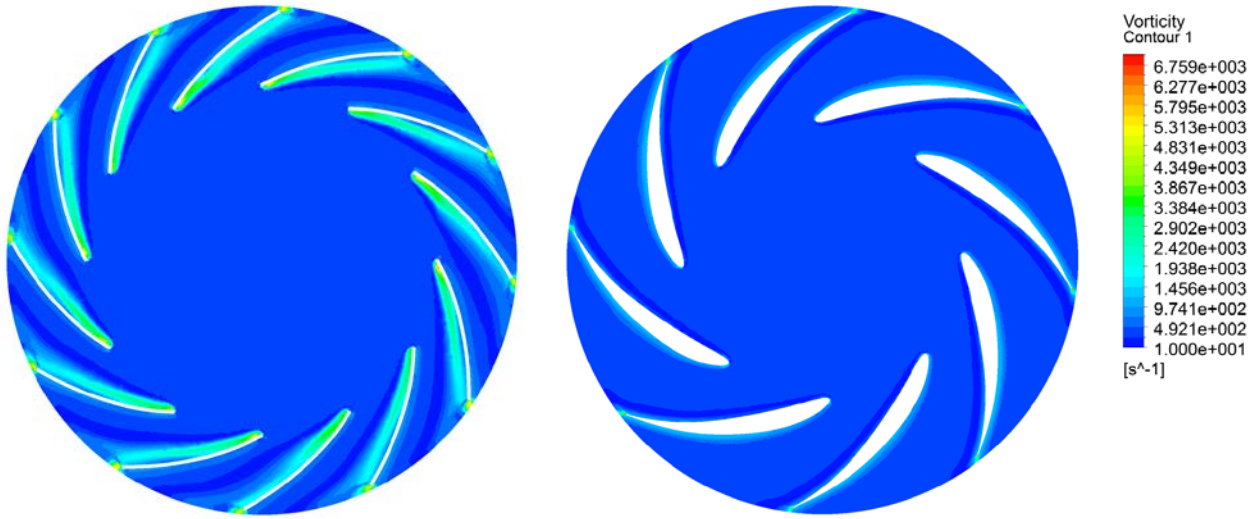

(a) Original Model (b) Optimized Model

Fig. 12 Vortices contour at the rated flow coefficient

Figure 13 shows the relative velocity distribution at the outlet of the passage in the middle section of the impeller. The abscissa indicates the position from pressure surface to suction surface. It can be seen in the Fig.13 (a) that the jet-wake pattern exists in both original and optimized models, but the jet-wake pattern in the optimized model is weaker than that in the original model. It is obvious in the Fig.13 (b) that the jet-wake pattern in the optimized model is inhibited at the flow coefficient of 0.164. In the meantime, the maximum relative velocity of optimized model is lower. This means that the kinetic energy loss of optimized model at this flow coefficient is less than that of the original model. It can be seen in Fig.13 (c) that there is no distinct difference of the maximum value of relative velocity between the original and optimized models. But there is an obvious jet-wake pattern exists in the original model, and the relative velocity near the pressure surface is higher than that near the suction surface. This is because the main flow is influenced by the separation that occurs on the suction surface, and then the relative velocity near the suction surface reduces. The relative velocity at the outlet of the optimized model is more uniform. Thus, the flow in the optimized model is improved. Fig.13 (d) shows the relative velocity distribution at the flow coefficient of 0.284. It can be seen that in the optimized model, the relative velocity is higher than that in the original model, which means that there is more kinetic energy loss in the optimized model. In the optimized model, the relative velocity near the suction surface is higher than that near the pressure surface, but in the original model, the relative velocity distribution is more uniform. This is the reason why the original model can get high efficiency at high flow coefficient.

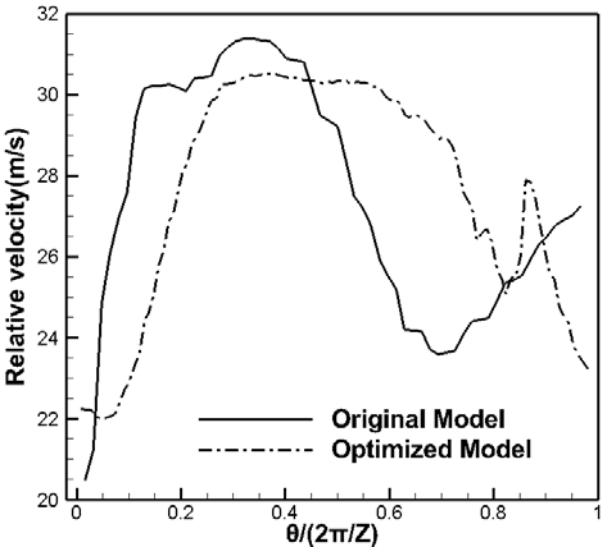

Fig. 13(a) Relative velocity distribution on passage outlet at the the flow coefficient of 0.115

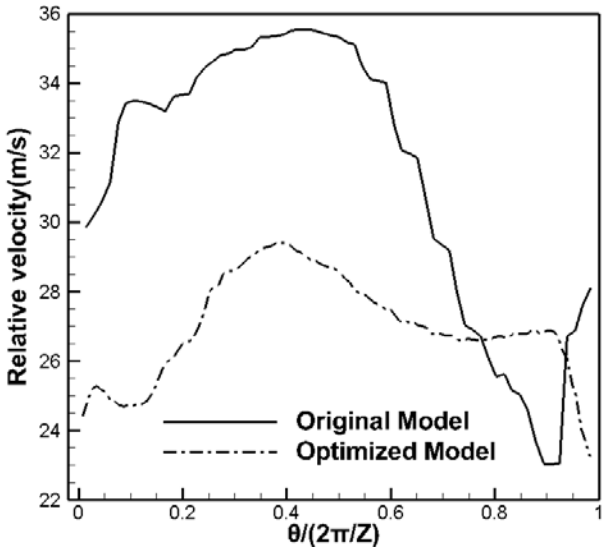

Fig. 13(b) Relative velocity distribution on passage outlet at the flow coefficient of 0.164

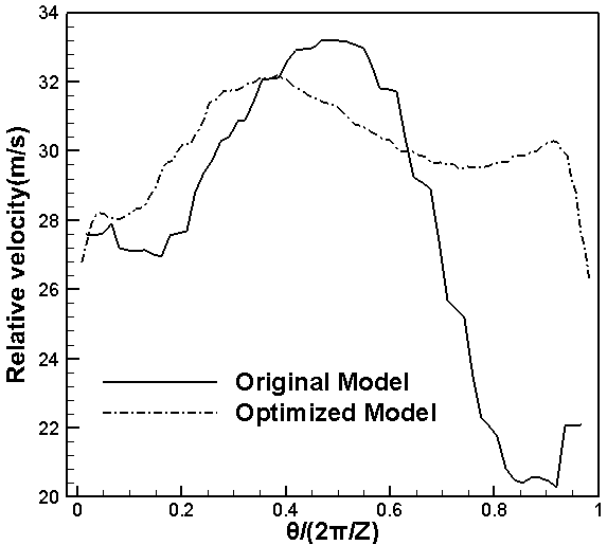

Fig. 13(c) Relative velocity distribution on passage outlet at the rated flow coefficient

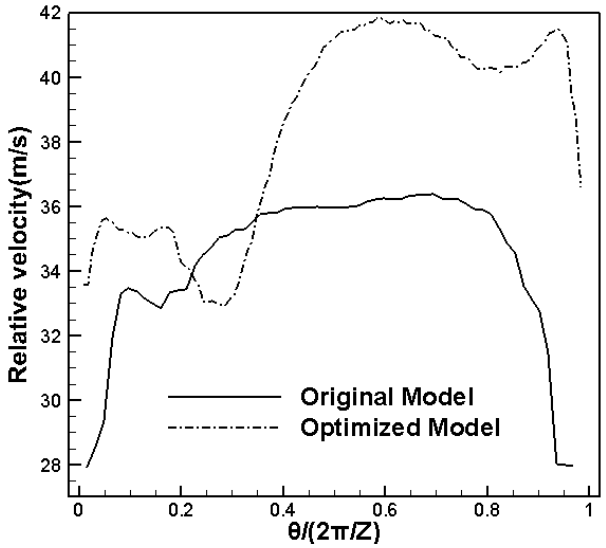

Fig. 13(d) Relative velocity distribution on passage outlet at the flow coefficient of 0.283

Figure 14 shows the streamline on the middle section of the impeller of both original and optimized model at the flow coefficient of 0.164. It can be seen that the at this flow coefficient, the vortex occurred in the channel because of the flow separation on the suction surface. But in the optimized model, the flow separation is inhibited effectively and there is no vortex at this flow coefficient.

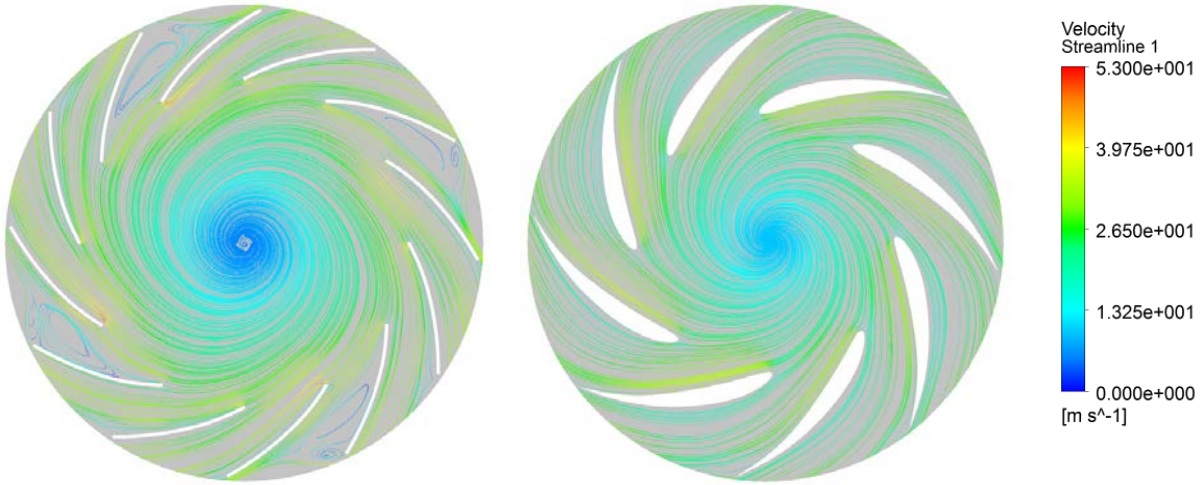

(a) Original Model (b) Optimized Model

Fig. 14 Streamline on the middle section at the flow coefficient of 0.164

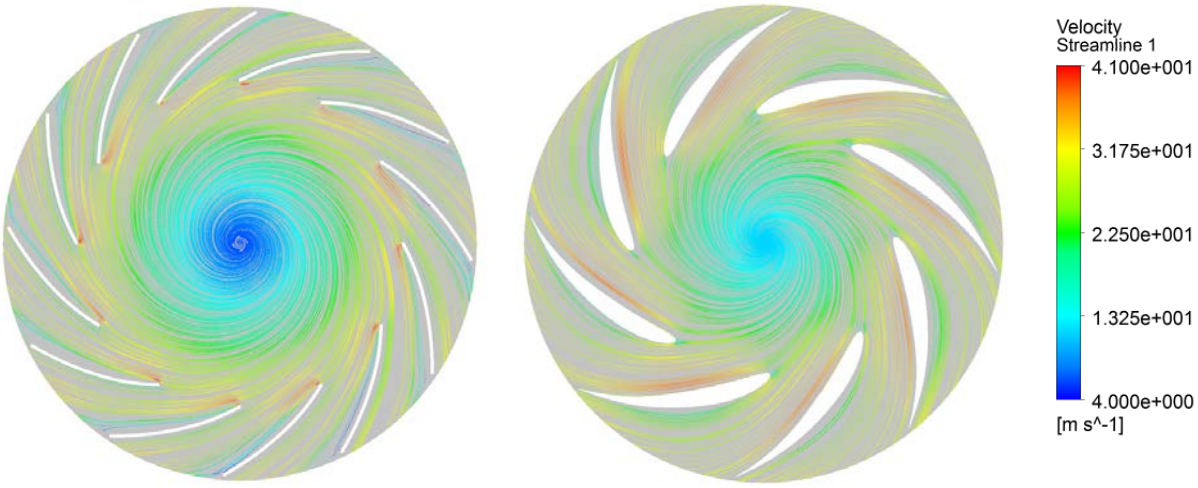

(a) Original Model (b) Optimized Model

Fig. 15 Streamline on the middle section at the rated flow coefficient

Figure 15 is the streamline on the middle section of the impeller of both original and optimized model at the rated flow coefficient. It can be seen that in the original model, there is flow separation on the suction surface outlet. But in the optimized model, there is no flow separation. This means the flow performance is improved in the optimized model.

Figure 16 is the static pressure distribution on the radial section. It can be seen that a low pressure area exists near the suction surface in the original model, and this area is also near the shroud. There is a pressure gradient between the suction and pressure surface. The flow inside the boundary layer will be forced by this pressure gradient, and then the secondary flow occurs. The secondary flow will thicken the boundary layer thickness and trigger more loss. In the optimized model, the low pressure area is smaller, and the secondary flow is improved.

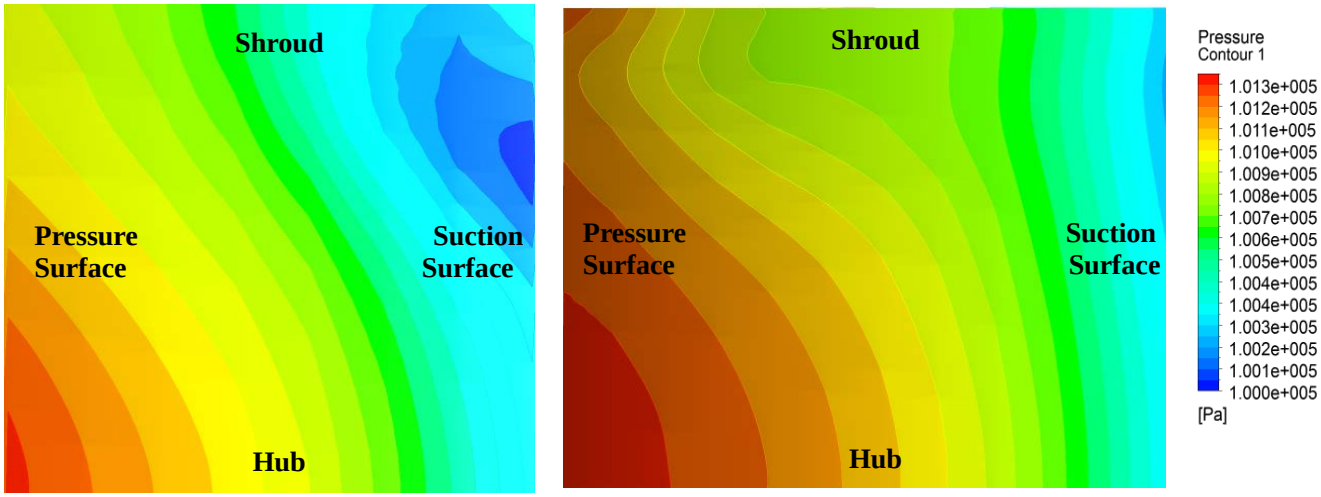

(a) Original Model (b) Optimized Model

Fig. 16 Static pressure distribution on the radial section at the rated flow coefficient

7. Conclusions

In this paper, the controlling velocity distribution method is employed to optimize the blade design of a centrifugal impeller. The incompressible 3D N-S equation is applied to predict the performance of original and optimized models. The numerical results of original model are in good agreement with the experimental data. The conclusions are summarized as follow:

1. The performance of plenum fan can be improved distinctly by controlling the velocity distribution, and both the static pressure and the static pressure efficiency have been increased. The pressure loss at the blade outlet is less than that of the original model except at high flow coefficient.

2. The flow in the optimized model is improved distinctly. The boundary layer separation on the suction surface has been inhibited and the stability of plenum fan has been improved. The flow at the impeller outlet is also studied, and the jet-wake pattern at the impeller outlet is improved obviously by optimization.

Acknowledgments

This work is supported by the Natural Science Foundation of China (51579224), the Natural Science Foundation of Zhejiang Province (LY14E060003), Zhejiang Province Key Science and Technology Innovation Team Project (2013TD18), Special Major Project of Science and Technology of Zhejiang Province (2013C01139), and Graduate Student Innovation Research Project of Zhejiang Sci-Tech University (YCX14032).

References

[1] Polanský, J., Kalmár, L., and Gášpár. R., 2013, “Prediction of Dynamic and Aerodynamic Characteristics of the Centrifugal Fan with Forward Curved Blades.” Journal of Thermal Science, Vol. 22, No. 6, pp. 517-521.
[2] Kim, J. H., Cha, K. H., Kim, K. Y., and Jang, C. M., 2012, “Numerical Investigation on Aerodynamic Performance of a Centrifugal Fan with Splitter Blades,” International Journal of Fluid Machinery and System, Vol. 5, No. 4, pp. 168-173.
[3] Dundi, T. M. K., Sitaram, N., and Suresh. M., 2012, “Application of Gurney Flaps on a Centrifugal Fan Impeller,” International Journal of Fluid Machinery and System, Vol. 5, No. 2, pp. 65-71.
[4] Hariharan, C., and Govardhan, M., 2013, “Effect of Inlet Clearance Gap on the Performance of an Industrial Centrifugal Blower with Parallel Wall Volute,” International Journal of Fluid Machinery and System, Vol. 6, No. 3, pp. 113-120.
[5] Oh, H. W., Yoon, E. S., and Chung, M. K., 1997, “An optimum set of loss models for performance prediction of centrifugal compressors,” Proceedings of the Institution of Mechanical Engineers Part A Journal of Power and Energy, Vol. 211, No. 4, pp. 331-338.
[6] Kim, J. H., Choi, J. H., Husain, A., and Kim, K. Y., 2010, “Multi-objective optimization of a centrifugal compressor impeller through evolutionary algorithms,” Proceedings of the Institution of Mechanical Engineers Part A Journal of Power and Energy, Vol. 224, No. 5, pp. 711-721.
[7] Stanitz, J. D. and Prian, V. D., 1951, a Rapid Approximate Method for Determining Velocity Distribution on Impeller Blades of Centrifugal Compressors, NACA TN2421.
[8] Johnson, M. W. and Moore, J., 1980, “The Development of Wake Flow in a Centrifugal Impeller,” Journal of Engineering for Gas Turbines and Power, Vol. 102, No. 2, pp. 382-389.
[9] Galerkin, Y. B., Zuev, A. V., Seleznev, K. P., and Strizhak, L. Y., 1973, “Test designing centrifugal compressor wheels according to a stated velocity distribution,” Chemical and Petroleum Engineering, Vol. 9, No. 4, pp. 306-312.
[10] Balje, O. E., 1970, “Loss and Flow Path Studies on Centrifugal Compressors—Part I,” Journal of Engineering for Gas Turbines and Power, Vol. 92, No. 3, pp. 275-286.
[11] Qi, D. Y. and Li, Z. L., 1994, “A Simple Two-Dimensional inverse Design Method for the Impeller Blades of Centrifugal Fans,” Chinese Journal of Applied Mechanics, Vol. 11, No. 3, pp. 98-102.
[12] Li, J. Y., Niu, Z. N., and Liang, Y. X., 2009, “Design of 2D Blade Curves of Centrifugal Fans by Controlled Deceleration Flow Method,” Journal of Xi’an Jiaotong University, Vol. 43, No. 9, pp. 67-70.
[13] Yagi, M., Kishibe, T., Shibata, T., Nishida, h., and Kobayashi, H., 2008, “Performance Improvement of Centrifugal Compressor Impellers by Optimizing Blade-Loading Distribution,” ASME Turbo Expo, Berlin, Germany, GT2008-51025
[14] Shibata, T., Yagi, M., Nishida, H., Kobayashi, H., and Tanaka, M., 2010, “Performance Improvement of a Centrifugal Compressor Stage by Increasing Degree of Reaction and Optimizing Blade Loading of a 3D Impeller,” Journal of Turbomachinery, Vol. 133, No. 2, pp. 021004-1-021004-8.
[15] Lin, S. C. and Huang, C. L., 2002, “An integrated experimental and numerical study of forward–curved centrifugal fan, Experimental Thermal and Fluid Science,” Vol. 26, No. 5, pp. 421-434.
[16] White, F. M., 2006, Viscous Fluid Flow, McGraw-Hill, New York.